Carcinogenesis, 2019, 1–14

doi:10.1093/carcin/bgz011
Advance Access publication February 1, 2019
Original Article

ORIGINAL ARTICLE

MicroRNA-708 activation by glucocorticoid receptor agonists regulate breast cancer tumorigenesis and metastasis *via* downregulation of NF-κB signaling

K.J.Senthil Kumar[1,2], M.Gokila Vani[1,2], Hen-Wen Hsieh[3], Chin-Chung Lin[3], Jiunn-Wang Liao[4], Pin-Ju Chueh[5,6], and Sheng-Yang Wang[1,2,7,*]

[1]Department of Forestry, National Chung Hsing University, Taichung, Taiwan, [2]National Chung Hsing University/University of California at Davis, Plant and Food Biotechnology Center, National Chung Hsing University, Taichung, Taiwan, [3]Taiwan Leader Biotech Company, Taipei, Taiwan, [4]Graduate Institute of Veterinary Pathology, National Chung Hsing University, Taichung 402, Taiwan, [5]Institute of Biomedical Sciences, National Chung Hsing University, Taichung, Taiwan, [6]Department of Biotechnology, Asia University, Taichung, Taiwan, and [7]Agricultural Biotechnology Research Center, Academia Sinica, Taipei, Taiwan

*To whom correspondence should be addressed. Tel: +886-4-22840345 ext. 138; Fax: +886-422873628; Email: taiwanfir@dragon.nchu.edu.tw

Abstract

Therapeutic administration of glucocorticoids (GCs) is frequently used as add-on chemotherapy for palliative purposes during breast cancer treatment. Recent studies have shown that GC treatment induces microRNA-708 in ovarian cancer cells, resulting in impaired tumor cell proliferation and metastasis. However, the regulatory functions of GCs on miR-708 and its downstream target genes in human breast cancer cells (BCCs) are poorly understood. In this study, we found that treatment with either the synthetic GC dexamethasone (DEX) or the natural GC mimic, antcin A (ATA) significantly increased miR-708 expression by transactivation of glucocorticoid receptor alpha (GRα) in MCF-7 and MDA-MB-231 human BCCs. Induction of miR-708 by GR agonists resulted in inhibition of cell proliferation, cell-cycle progression, cancer stem cell (CSC)-like phenotype and metastasis of BCCs. In addition, GR agonist treatment or miR-708 mimic transfection remarkably inhibited IKKβ expression and suppressed nuclear factor-kappaB (NF-κB) activity and its downstream target genes, including *COX-2*, *cMYC*, *cyclin D1*, Matrix metalloproteinase *(MMP)-2*, *MMP-9*, CD24, CD44 and increased $p21^{CIP1}$ and $p27^{KIP1}$ that are known to be involved in proliferation, cell-cycle progression, metastasis and CSC marker protein. BCCs xenograft models indicate that treatment with GR agonists significantly reduced tumor growth, weight and volume. Overall, our data strongly suggest that GR agonists induced miR-708 and downstream suppression of NF-κB signaling, which may be applicable as a novel therapeutic intervention in breast cancer treatment.

Introduction

Breast cancer is the most frequent malignancy and leading cause of cancer-related death in women worldwide. Approximately 1.3 million new cases of breast cancer are diagnosed annually and the disease is associated with an estimated 0.5 million deaths (1). According to a report by the International Agency for Research on Cancer, breast cancer accounts for 11.88% of all cancer making it the second most common malignancy worldwide (2). These statistics highlight the urgent need for improvements in detection, diagnosis, and treatment of breast cancer.

Glucocorticoids (GCs) are a class of corticosteroids known to exert pronounced effects on metabolism, survival, proliferation and differentiation of cells. Most, if not all, of these actions are mediated through the glucocorticoid receptor (GR), a member of the nuclear receptor superfamily of transcription factors

Received: September 4, 2018; **Revised:** January 6, 2019; **Accepted:** January 22, 2019

Abbreviations

BCC	breast cancer cell
CDK	cyclin-dependent kinase
CSC	cancer stem cell
DEX	dexamethasone
FBS	fetal bovine serum
FITC	fluorescein isothiocyanate
GC	glucocorticoid
GRα	glucocorticoid receptor alpha
mRNA	messenger RNA
miRNA	microRNA
MMP	Matrix metalloproteinase
NF-κB	nuclear factor-kappaB
PBS	phosphate-buffered saline
RT	reverse transcription
siRNA	small interfering RNA
TGF	transforming growth factor
TNBC	triple-negative breast cancer
3′UTR	3′-untranslated region

(3). GCs are corticosteroids that bind to the GR that is present in almost all vertebrate animal cells (4). Synthetic GCs, such as dexamethasone (DEX), betamethasone, prednisone and methylprednisolone, are widely used as anti-inflammatory drugs. Indeed, DEX is frequently used as a pretreatment during chemotherapy in many cancer types to prevent a hypersensitivity reaction (5). An increasing number of *in vitro* and *in vivo* studies suggest that DEX attenuates tumor growth and induces apoptosis in prostate cancer (6), melanoma (6) and several malignant lymphoid cancers (7). A recent study showed that GR antagonist mifepristone increases paclitaxel sensitivity in triple-negative breast cancer (TNBC) cell lines, whereas mifepristone treatment alone had no effect on TNBC viability or colonogenicity in the absence of chemotherapy *in vitro* (8) and pretreatment of xenograft tumors with DEX results in significant inhibition of the therapeutic efficacy of paclitaxel *in vivo* (9), raising efficacy concerns. To date, no prospective investigation has assessed the effect of GC agonists on tumor growth, cancer stem cell (CSC) differentiation and metastasis of breast cancers. Therefore, further studies are warranted to clarify the exact roles and the application of GC in breast cancer therapy.

GR agonist-induced apoptosis and tumor growth appears to be a complicated process involving multiple signaling pathways. They include negative regulation of survival, proliferation and cell-cycle regulatory genes such as *COX-2*, *cMYC* and *cyclin D1* that act through a *trans*-repression mechanism of nuclear factor-kappaB (NF-κB) and transactivation of apoptosis inducing genes, including Bim1 (7). NF-κB, a transcription factor that belongs to the Rel family, plays critical roles in survival, proliferation, differentiation, inflammation and immunity. A frequent feature found in most breast cancer tumors is the constitutive activation of NF-κB, deregulated NF-κB activation results in persistent nuclear localization of proteins such as p50, p52, p65, cRel and RelB, which disrupt the balance between cell proliferation and death through the upregulation of anti-apoptotic genes (10). CSCs or tumor initiating stem-like cells are a small subset of tumor-initiating cells, which are capable of self-renewal and resist various chemotherapeutic drugs. CSCs have been identified in various cancers including brain, breast, ovarian, prostate, pancreatic and colon (11). Several signaling pathways have been implicated in the self-renewal behavior of breast CSCs, including Wnt/β-catenin, Notch, Hedgehog and NF-κB pathways (12). Among them, NF-κB has received attention, because it is a frequent feature found in most breast cancer tumors and the constitutive activation of NF-κB plays a critical role in self-renewal of breast CSCs (13). However, the molecular mechanism by which GR agonist-mediated suppresses NF-κB and breast CSCs regulation occurs has yet to be elucidated.

MicroRNAs (miRNAs), a class of endogenous and small non-coding RNA molecules, are about 22 nucleotides in length and are commonly found in plants, animals and virus genomes that function in RNA silencing and post-transcriptional regulation of gene expression. miRNA can directly bind to the 3′-untranslated region (3′UTR) of transcripts that repress translation and/or induce messenger RNA (mRNA) degradation in various biological processes (14), including cancer cell proliferation, metastasis, CSC differentiation and other biological functions (15). The discovery of miRNAs has provided new insights in cancer research. miRNA regulation in breast cancer was first reported in 2005 and demonstrated that 29 miRNAs were differentially expressed in breast tumor tissues compared with normal breast tissues (16). miR-708, a newly identified miRNA, has been reported to suppress cancer progression in certain types of cancers, including renal cell carcinoma, hepatocellular carcinoma, ovarian carcinoma, prostate carcinoma, breast carcinoma, glioblastoma multiforme and Ewing's sarcoma. However, in few cancer types, miRNA serves as an oncogenic miRNA, especially in bladder carcinoma, colorectal carcinoma and certain lung carcinoma (17). A recent study reported that epigenetic silencing of miR-708 enhances NF-κB signaling by directly targeting IKKβ in chronic lymphocytic leukemia (18). A follow-on study by Ma et al. (2015) found that forced expression of miR-708 suppressed proliferation and invasive ability of TNBC cells *via* targeting lysine-specific histone demethylase (LSD1) *in vitro* (19). However, only a few studies have looked at the functions of miR-708 in breast carcinoma and the molecular regulatory mechanisms are largely unexplored.

Synthetic GR agonists are widely used as an adjuvant treatment during chemotherapy, whereas naturally occurring GR agonists or phytosteroids are poorly studied. Phytosteroids are potential modulators of inflammation and the immune system (20). We reported previously that Antcin A (ATA), a steroid-like phytochemical isolated from the medicinal mushroom of *Antrodia cinnamomea*, inhibits inflammation in lung cells *via* mimicking a GR agonist, and this effect was highly comparable with synthetic GR agonists, such as cortisone and DEX (21). In addition, a little is known about the regulation of miRNAs through the GR agonist-mediated signaling pathways in breast cancer. In the present study, we report the finding that both synthetic and naturally occurring GR agonists play a suppressive role in breast cancer tumorigenesis and metastasis *via* induction of miR-708. Activation of miR-708 through GRα transactivation results in decreased breast cancer cell (BCC) proliferation and induces cell-cycle arrest mainly through transcriptional repression of NF-κB and its target genes, *COX-2* and *cMYC*.

Materials and methods

Chemicals and reagents

Antcin A (ATA) was isolated from the fruiting bodies of *A. cinnamomea* as described previously (21). The purity of ATA was above 99% according to high-performance liquid chromatography and ^{1}H-NMR analyses. Dulbecco's modified Eagle's medium, RPMI medium, minimum essential medium, fetal bovine serum (FBS), sodium pyruvate, penicillin and streptomycin were obtained from Invitrogen (Carlsbad, CA). DEX, 3-(4,5-dimethyl-thiazol-2-yl)-2,5-diphenyl tetrazolium bromide, 2-(4-amidinophenyl)-1H-indole-6-carboxamidine and cycloheximide were

purchased from Sigma–Aldrich (St. Louis, CA). Small interfering RNAs (siRNAs) were obtained from Cell Signaling Technology (Danvers, MA). List of antibodies used in this study was summarized in Supplementary Table 1, available at *Carcinogenesis* Online. All other chemicals were reagent grade or high-performance liquid chromatography grade and supplied by either Merck (Darmstadt, Germany) or Sigma–Aldrich.

Cell culture, sample treatment and transfection

The human breast normal and carcinoma cell lines MCF-10A, MCF-7 and MDA-MB-231 were obtained from Bioresource Collection and Research Center, Hsinchu, Taiwan, and authenticated by short tandem repeat PCR profiling at Bioresource Collection and Research Center. The cell lines were obtained in March 2015 and immediately cultured for experiments. MCF-10A, MCF-7 and MDA-MB-231 cells were grown in Dulbecco's modified Eagle's medium/Ham's-F12, minimum essential medium and RPMI medium, respectively, and supplemented with 10% FBS, 1.5 g/l sodium bicarbonate and 100 U/l penicillin and streptomycin at 37°C in a humidified atmosphere of 5% CO_2. Cells were treated with DEX (1 μM) or ATA (10 μM) for 24–72 h. On the other hand, cells were transfected with siRNA or miRNA mimic using Lipofectamine 2000 (Invitrogen). Twenty nanomolars were used for each pre-miRNA or siRNA transfection. Cells were stimulated with 20 ng/ml of tumor necrosis factor -α. Controls were performed in the presence of media with 0.1% dimethyl sulfoxide.

Cell proliferation and Cell-cycle analyses

Cell proliferation was determined by a commercially available proliferation assay kit (CellTiter 96® AQ_{ueous} One Solution Cell Proliferation Assay, Promega, Madison, WI). Cell-cycle progression was measured by flow cytometry. Briefly, cells were grown in six-well plates at a density of 1 × 10^5 cells per well and treated with pre-miR-708 or DEX and ATA for 72 h. After treatment, cells were collected and then centrifuged for 3 min at 1500 × g. Cells were fixed with 95% cold ethanol and kept at –20°C overnight. The cell pellet was washed again with phosphate-buffered saline (PBS) and centrifuged at 1500*g* for 3 min, permeabilized with 1 ml PI/Triton X-100 (20 μg/ml PI, 0.1% Triton X-100 and 2.5 μg/ml RNAse) and incubated on ice for 30 min. The total cellular DNA content was analyzed with a flow cytometer (Beckman Coulter FC500) by acquiring at least 10 000 events. The analysis of the cell cycle was performed by using CXP software (Beckman Coulter, Brea, CA).

Flow cytometric analysis of CD44 and CD24 expression

MDA-MB-231 and MCF-7 cells were incubated with DEX or ATA for 24 h. On the other hand, cells were transfected with pre-miR-708. After treatment, cells were collected by trypsinization and 1 × 10^6 cells were incubated with 2 μg/ml (1:10) of anti-CD44-APC and anti-CD24-FITC antibodies (BD Biosciences, San Jose, CA) in the dark, on ice, for 30 min, washed twice with cold PBS, then resuspended in PBS (1 ml). CD44+CD24- and CD44-CD24+ cells were sorted with a flow cytometer (Beckman Coulter FC500) by acquiring at least 10 000 events. The analysis of the $CD44^+$ and $CD24^+$ cells were performed by using CXP software (Beckman Coulter).

Tumor-sphere formation assay

To measure the tumor sphere formation of BCCs, 200 μl of Matrigel (BD Biosciences) were spread as a thick layer on a six-well plate and allowed to polymerize at 37°C for 15 min. For each well, 5 × 10^4 cells per well were suspended in 1 ml of 10% Matrigel in minimum essential medium or Dulbecco's modified Eagle's medium (10% FBS) for MCF-7 and MDA-MB-231, respectively. Plates were incubated at 37°C to allow cells to fully settle before the media were replaced with appropriate culture media containing 5% Matrigel. Both layers were supplemented with DEX or ATA or vehicle (0.1% dimethyl sulfoxide). Cells were grown for 15 days; fresh growth media with Matrigel was replenished every 3 days. Images of representative fields were taken at day 15.

In vitro migration and invasion assay

MCF-7 or MDA-MB-231 at a density of 1 × 10^5 cells per well were seeded into a 12-well culture plate with a silicon cell-free gap insert (ibidi GmbH, Martinsried, Germany). After monolayer formation, the insert was removed, washed with PBS and then cells were treated with DEX or ATA for 24 h. To induce MCF-7 cell migration, 20 ng/ml of transforming growth factor (TGF)-β1 was added to the culture media ($MCF\text{-}7^{TGF\text{-}\beta}$) for 2 h prior to sample treatment. The migrated cells were photographed (×100 magnification) at 0 and 24 h to monitor the migration of cells into the wounded area, and the closure of the wounded area was calculated. During wound healing assay, cell migration significantly interferes with cell proliferation. Therefore, serum starving is the most non-pharmacological method for minimizing cell proliferation. In the present study, we performed wound heling assay with serum-free (serum starvation) medium. To determine the tumor cell invasion, Matrigel invasion assay was performed in 24-well *trans*-well culture plates. BD Matrigel Basement Membrane Matrix (10 μl, 0.5 mg/ml; BD Bioscience) was applied to 8-μm polycarbonate membrane filters, and 1 × 10^5 cells were seeded to the Matrigel-coated filters in 200 μl of serum-free medium containing DEX or ATA in triplicate. The bottom chamber of the apparatus contained 750 μl of complete growth medium. Cells were allowed to migrate for 24 h at 37°C. The invasive cells on the bottom side of the membrane were fixed in cold methanol for 15 min and washed three times with PBS. The cells were stained with Giemsa stain solution and then destained with PBS. Images were obtained using an optical microscope (×200 magnification), and invading cells were quantified by manual counting. For gene silencing, prior to the experiment, cells were transfected with scrambled siRNA or siGRα.

Immunofluorescence

Immunofluorescence analysis was performed as described previously (22). Briefly, MCF-7 and MDA-MB-231 cells seeded at a density of 1 × 10^4 cells per well in an eight-well glass Nunc Lab-Tek chamber (Thermo Fisher Scientific, Waltham, MA), and DEX and ATA are transfected with miR-708 mimic for 72 h. After treatment, culture media was removed and cells were fixed in 4% paraformaldehyde for 15 min, permeabilized with 0.1% Triton X-100 for 10 min, washed and blocked with 10% FBS in PBS, and then incubated overnight with the corresponding primary antibodies in 1.5% FBS. The cells were then incubated with fluorescein isothiocyanate (FITC)-conjugated secondary antibody for another 1 h in 6% bovine serum albumin. Then, the cells were stained with 1 μg/ml 2-(4-amidinophenyl)-1H-indole-6-carboxamidine (Cell Signaling Technology) for 5 min, washed with PBS and visualized using a fluorescence microscope (Motic Electric Group) at ×40 magnification.

Protein extraction and immunoblotting

Control and treated cells were lysed in either RIPA lysis buffer or nuclear and cytoplasmic extraction reagents (Thermo Fisher Scientific) or transmembrane protein extraction reagent (Fivephoton Biochemicals, San Diego, CA) following the manufacturer's protocol. Protein content was determined by Bio-Rad protein assay reagent (Bio-Rad Laboratories, Hercules, CA). Equal amounts of denatured protein samples (60 μg) were separated by 7–12% sodium dodecyl sulfate-poly acrylamide gel electrophoresis and the separated proteins were transferred onto polyvinylidene chloride membrane overnight. The transferred protein membranes were incubated with specific primary antibodies overnight and inoculated with either horseradish peroxidase-conjugated goat anti-rabbit or anti-mouse antibodies for 2 h. The blots were developed with enhanced chemiluminescence western blotting reagent (Millipore, Billerica, MA) and the luminescence signals were detected by using VL Chemi-Smart 3000 (Viogene Biotek, Sunnyvale, CA).

Quantitative real-time PCR

Total RNA was extracted by using Trizol Reagent (Thermo Fisher Scientific). RNA concentration was quantified with a NanoVue Plus spectrophotometer (GE Health Care Life Sciences, Chicago, IL). Real-time PCR was performed on a real-time PCR detection system and software (Applied Biosystems, Foster City, CA). First-strand complementary DNA was generated by SuperScript III reverse transcriptase kit (Invitrogen). Quantification of mRNA expression for genes of interest was performed by qPCR reactions were performed with equal volume of complementary DNA, forward and reverse primers (10 μM), power SYBR Green Master Mix (Applied Biosystems). The mRNA levels were normalized with glyceraldehyde 3-phosphate dehydrogenase, whereas miRNA levels were normalized with U6. The primer sequences of each gene for qPCR are summarized in Supplementary Table 2, available at *Carcinogenesis* Online.

Luciferase assay

The transcriptional activity of GRα and NF-κB were determined by commercially available luciferase reporter assay kits (GAL4 reporter kit, BPS Biosciences, San Diego, CA, and Cignal NF-κB pathway reporter assay kit, Quiagen, Chatsworth, CA). In 3′UTR reporter assay, BCCs were transfected with the pGL3-IKKβ 3′UTR, Renilla, together with or without pre-miR-708 or in the presence or absence of DEX and ATA, and then, the reporter activity was determined by dual-luciferase reporter assay system (Promega). Primer sequences used are provided in Supplementary Table 3, available at *Carcinogenesis* Online.

Animal and tumor cell inoculation

Four-week-old female athymic nude mice (BALB/c-nu) were purchased from BioLASCO Taiwan (Taipei, Taiwan) and were maintained in caged housing separately in a specifically designed pathogen-free isolation facility with a 12 h light and 12 h dark cycle; the mice were provided rodent chow (Oriental Yeast, Tokyo, Japan) and water *ad libitum*. All animal experiments were conducted in accordance with the *Guide for the Care and Use of Laboratory Animals* and Taiwan laws relating to the protection of animals and were approved by the local ethics committee. For tumor cell inoculation, MCF-7 and MDA-MB-231 cells at a density of (1×10^6 cells in 200 µl matrix gel) were subcutaneously injected into the right-hind flank of nude mice. Experiments were carried out using cells at a passage number of <15. Mice were divided into six groups consisting of five mice each. When the mean tumor volume was 50 mm^3 (~3 weeks after tumor inoculation), treatment was initiated. The four study groups (MCF-7_DEX, MCF-7_ATA, MDA-MB-231_DEX and MDA-MB-231_ATA) received intraperitoneal injections of either DEX (0.1 mg/kg) or ATA (10 mg/kg) in PBS buffer twice a week for 10 weeks, whereas the control groups (MCF-7_PBS and MDA-MB-231_PBS) received vehicle only (PBS). The experimental period was 10 weeks, following 7 weeks of drug administration. After 10 weeks of treatment, the mice were killed. The tumors were removed, photographed and weighed before fixing in 4% paraformaldehyde. Tumor volume, as determined by caliper measurements of tumor length, width and depth, were calculated using the formula: length × $width^2$ × height ×1/2 of every three consecutive days. To monitor drug toxicity, the body weight of each animal was measured every 3 days.

Histopathology and immunohistochemistry analysis

Biopsied tumor tissues were embedded in paraffin and cut into 3 mm thick sections and stained with hematoxylin–eosin for light microscopy analysis. Surviving tumor cells, necrosis and apoptosis were determined. To examine the expression of tumorigenic markers, tissue sections were immunohistochemically stained with anti-COX-2 and anti-NF-κB antibodies for 2 h at room temperature. The secondary detection antibody was conjugated to a REAL EnVision Detection System (Dako Cytomation A/S, Glostrup Denmark) .

Statistical data analysis

Data are expressed as mean ± standard deviation. All data were analyzed using the statistical software Graphpad Prism version 6.0 for Windows (GraphPad Software, La Jolla, CA). Statistical analysis was performed using one-way analysis of variance followed by Dunnett's test for multiple comparison, with a P-value of <0.05 indicating statistical significance.

Results

GR agonist activates miR-708 in BCCs via GRα signaling

To elucidate the differential expression of miR-708 in human normal and cancerous breast cells, we utilized a normal mammary gland epithelial cell line (MCF-10A), a non-malignant human breast adenocarcinoma (MCF-7) and a highly malignant human breast adenocarcinoma (MDA-MB-231) cell line. Results of reverse transcription (RT)–PCR analysis revealed that normal human breast epithelial cells (MCF-10A) exhibited higher level of miR-708 (11.11-fold), whereas reduced levels of miR-708 observed in both MCF-7 (2.43-fold) and MDA-MB-231 (0.43-fold) cell lines. In addition, further comparison of miR-708 expression in non-metastatic MCF-7 and highly metastatic MDA-MB-231 revealed that miR-708 expression was barely observed in MDA-MB-231 cells (Figure 1A). Further, transient transfection of miR-708 precursor resulted in miR-708 overexpression in both MCF-7 and MDA-MB-231 cells, as validated by RT-PCR (Figure 1B). A previous study reported that overexpression of miR-708 by transient transfection of miR-708 precursor decreased cell proliferation and invasion, whereas inhibition of miR-708 increased cell growth and metastasis of MDA-MB-231 cells (19). A recent study that searched for differential miRNA expression in ovarian cancer metastasis revealed that upregulation of miR-708 was associated with response to GR activation (23). Therefore, we hypothesized that GRα-mediated signaling may be involved in the regulation of miR-708 expression in breast carcinomas. To test the hypothesis, BCCs were incubated with DEX and ATA for 72 h, and the mRNA expression levels of miR-708 were determined by RT-PCR. As we expected, miR-708 expression levels were significantly increased by DEX and ATA (Figure 1C); whereas the increase of miR-708 expression by DEX and ATA were barely observed in GRα-silenced BCCs (Figure 1D). A similar result was also observed when BCCs were incubated with pharmacological inhibitor of GRα, mifepristone (Figure 1E) suggesting that GRα plays a functional role in the induction of miR-708. In addition, a dose–response curve of DEX on miR-708 expression revealed that over a dose of 500 nM significantly increased miR-708 expression in both MCF-7 and MDA-MB-231 cells, whereas low (1 nM) and high (100 nM) concentrations of DEX failed to induce miR-708 expression in BCCs (Supplementary Figure 1, available at *Carcinogenesis* Online). To further examine the *de novo* synthesis, BCCs were preincubated with protein synthesis inhibitor, CHX was then treated with DEX and ATA for 72 h. The result of RT-PCR analysis shows that in CHX-pretreated BCCs, treatment with DEX and ATA still increase the expression levels of miR-708 (Figure 1F). These data indicated that *de novo* protein synthesis is not required for DEX and ATA-induced GRα-mediated miR-708 transcriptions.

A previous report identified four potential promoter regions of miR-708 upon GC stimulation. Among them the promoter region-3 with a CpG Island, which is highly conserved among mammals, exhibited over 40-fold promoter activity in ovarian cancer cells (23). Therefore, we hypothesized that the promoter region-3 may serve as the promoter region for miR-708 in BCCs. We constructed a reporter plasmid carrying promoter-3 region and analyzed the transcriptional activity of GRα by luciferase reporter assay. As shown in Figure 1G, the luciferase activity was significantly increased to 8.2- and 6.5-fold in MCF-7 cells and 4.9- and 4.8-fold in MDA-MB-231 cells by DEX and ATA, respectively. This finding suggests that the transcriptional activity of GRα is responsible for miR-708 transcription upon GC stimulation. Next, we sought to examine the GC-mediated nuclear translocation of GRα. BCCs were treated with DEX and ATA for 48 h and then intercellular localization of GRα was examined by immunofluorescence analysis. In control cells, the basal levels of GRα were predominantly found in the cytoplasm and barely observed in the nucleus, whereas increased levels of GRα were recorded in the nucleus of BCCs after treatment with DEX or ATA (Figure 1H). Further confirmation with western blot analysis showed a similar result, i.e. that treatment with DEX and ATA significantly increased GRα levels in the nucleus, which is directly proportional to the reduction of GRα in the cytoplasm (Figure 1I), suggesting that GC-induced transcriptional

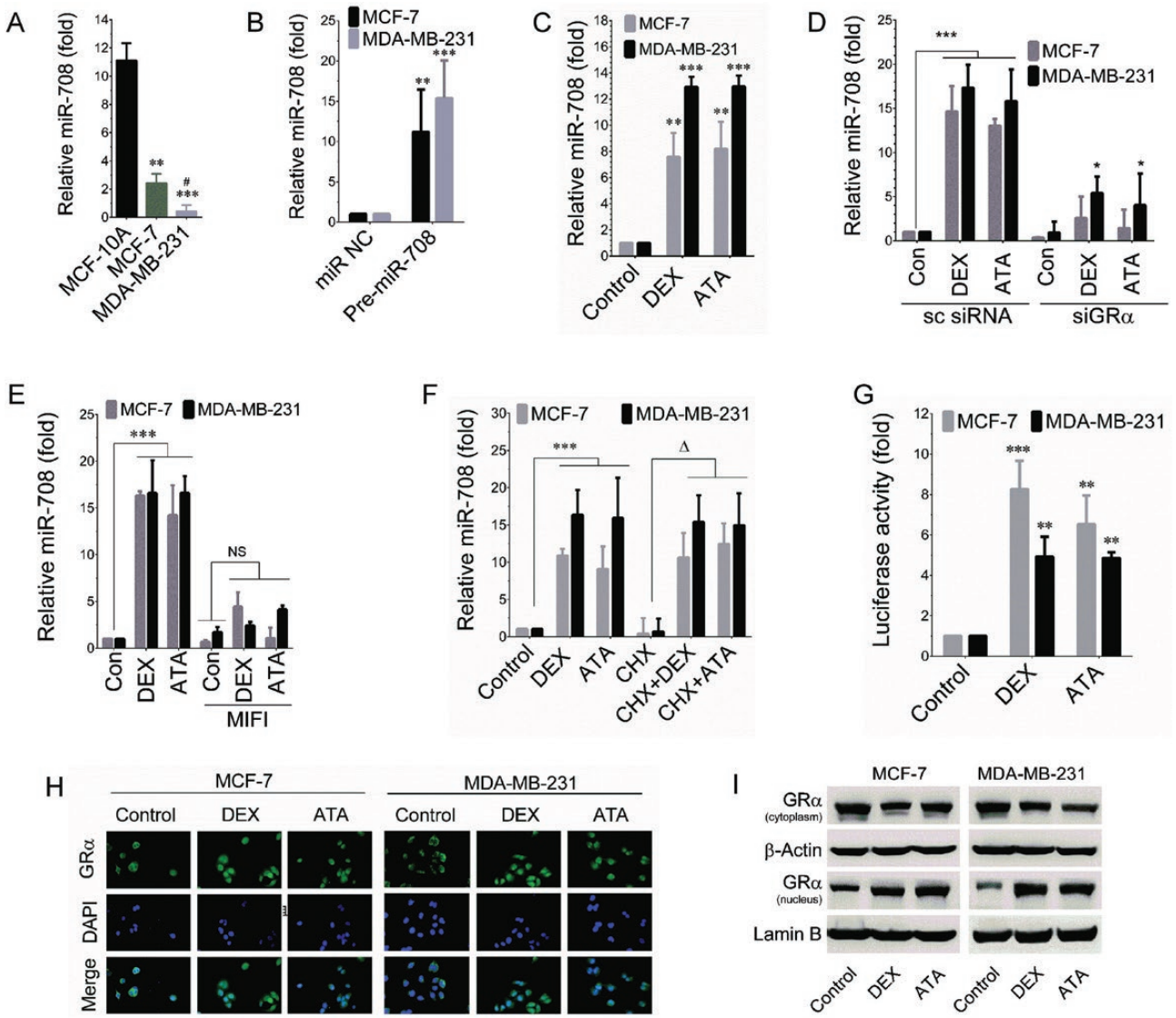

Figure 1. GR agonist activates miR-708 in BCCs *via* GRα signaling. **(A)** Quantitative RT-PCR analysis of miR-708 in normal, non-malignant and malignant human breast cell lines. **(B)** Expression of miR-708 in BCCs after transfection by pre-miR-708 for 72 h. **(C)** Expression of miR-708 in BCCs after treatment with DEX (1 μM) and ATA (10 μM) for 72 h. **(D)** Expression of miR-708 in BCCs transfected with scrambled siRNA (sc siRNA) or siRNA specific to GRα (siGRα) and then treated with DEX or ATA for 72 h. **(E)** BBCs were pretreated with mifepristone for 2 h and then treated with DEX or ATA for 72 h. The miR-708 expression was measured. **(F)** The miR-708 expression in BCCs pretreated with cycloheximide (CHX, 10 μM) for 12 h followed by DEX or ATA treatment for 72 h. The miR-708 level was normalized with U6. **(G)** Luciferase activity of GRα in BCCs after treatment with DEX or ATA for 48 h (RLU, relative luciferase unit). **(H)** Cellular localization of GRα in BCCs was measured by immunofluorescence after treatment with DEX or ATA for 48 h. 2-(4-Amidinophenyl)-1H -indole-6-carboxamidine was used to stain the nucleus. **(I)** The protein levels of GRα in the cytoplasm and the nucleus after treatment with DEX and ATA for 48 h. β-Actin and Lamin B1 served as internal controls for cytoplasmic and nuclear fractions. The data are reported as mean ± SD of three independent experiments. *P < 0.05, **P < 0.01 and ***P < 0.001 were significantly different from control versus pre-miR-708 transfection or DEX and ATA treatment groups.

activation of GRα is followed by a sequential event of its nuclear translocation.

MiRNA-708/GRα axis inhibits proliferation of BCCs

Next, to evaluate the functional role of GR agonists in BCCs, we examined the proliferation and stem-cell-like phenotype in the presence of DEX and ATA. In order to investigate the effects of GR agonists on BCCs, MCF-7 and MDA-MB-231 cells were incubated with various doses of DEX (0.1, 1, 2.5, 5 and 10 μM) and ATA (1, 5, 10 and 20 μM) for 24, 48 and 72 h. 0.1% of dimethyl sulfoxide served as a vehicle control. 3-(4,5-Dimethyl-thiazol-2-yl)-2,5-diphenyl tetrazolium bromide assay was used to analyze cell viability. We found that compared with the control group, treatment with DEX and ATA exhibited a sharp decline in the cell viability in a dose-and time-dependent manner (Supplementary Figure 2, available at *Carcinogenesis* Online). Indeed, treatment with DEX and ATA for 72 h showed significant reduction in cell number even at a low dose of ATA (1 μM). We then examined whether the reduction in cell number was associated with apoptotic cell death, apoptosis was determined by Annexin-V/PI staining. Results of flow cytometric analysis showed that there was no significant increase in apoptotic-positive cells in DEX or ATA treatment groups when compared with the control group (Supplementary Figure 3, available at

Carcinogenesis Online). Therefore, we hypothesized that GR agonists may induce growth arrest/senescence in BCCs, which may be the reason for the reduction in cell number. To test our hypothesis, MTS-based cell proliferation assay was performed. Results of the MTS assay showed that treatment with DEX and ATA significantly decreased the cell number, demonstrating the inhibitory effects of GR agonists on BCC proliferation (Figure 2A). In addition, the inhibitory effects of DEX and ATA were observed in a dose-dependent manner. Indeed, low concentrations of DEX (1–100 nM) increased cell proliferation without statistically significance in both MDA-MB-231 and MCF-7 cells, whereas a reduced cell proliferation was observed in MCF-7 cells at over a dose of 500 nm and 1000 nM in MDA-MB-231 cells (Supplementary Figure 4, available at *Carcinogenesis* Online). To further confirm whether inhibition of cell proliferation by GR agonists was mediated by miR-708, BCCs were transiently transfected with pre-miR-708 precursor and then cell proliferation was measured. As shown in Figure 2B, overexpression of miR-708 by pre-miR-708 significantly decreased percentage of viable cells suggesting that the inhibitory action of GR agonists on BCC proliferation was mediated by miR-708. Similar results were also observed in a parallel trypan blue exclusion assay (Supplementary Figure 5, available at *Carcinogenesis* Online).

We further analyzed cell-cycle progression by flow cytometer to confirm whether GR agonists inhibit cell proliferation by causing cell-cycle arrest. Results showed that treatment with DEX arrested both MCF-7 and MDA-MB-231cells at the G_2-M transition phase as evidenced by an increased cell population at the G_2 phase (Figure 2C). In contrast, the percentage of cell population in the G_0/G_1 phase was dramatically increased after treatment with ATA (Figure 2C), which indicated that DEX and ATA cause cell-cycle arrest at the G_2-M transition and G_1-S transition phase, respectively. This effect was further validated by transfection of pre-miR-708 in BCCs. In agreement with DEX treatment, transient transfection of pre-miR-708 arrested both MCF-7 and MDA-MB-231 cells at the G_2-M transition phase (Figure 2D). To further clarify these results, cell-cycle regulatory proteins, such as cyclins, cyclin-dependent kinases (CDKs) and CDK inhibitors were examined by immunoblotting. Our results strongly supported the above notion that G_1-S transition regulatory proteins, particularly cyclin D1, CDK4 and CDK6 were significantly downregulated by DEX and ATA (Figure 2E), whereas cyclin B and CDK1 were significantly inhibited by ATA (Figure 2E). However, the protein expression levels of cyclin A and cyclin E were unaffected by either DEX or ATA treatment in the tested BCCs. Interestingly, either treatment with DEX or ATA significantly upregulated $p21^{Cip1}$ and $p27^{Kip1}$ expression in both MCF-7 and MDA-MB-231 cells (Figure 2F). $p21^{Cip1}$ and $p27^{Kip1}$ are proteins that are frequently involved in growth arrest and cellular senescence.

MiRNA-708/GRα axis inhibits CSC-like phenotype in BCCs

Next, we examined whether GR agonists inhibit the formation of tumor spheres, a characteristic feature of CSC-like phenotype. To test this, BCCs were cultured in a three-dimensional microenvironment in the presence or absence of DEX and ATA for 14 days and then the number of multicellular tumor spheres formed under three-dimensional culture conditions were counted. MCF-7 and MDA-MB-231 cells formed tumor spheres

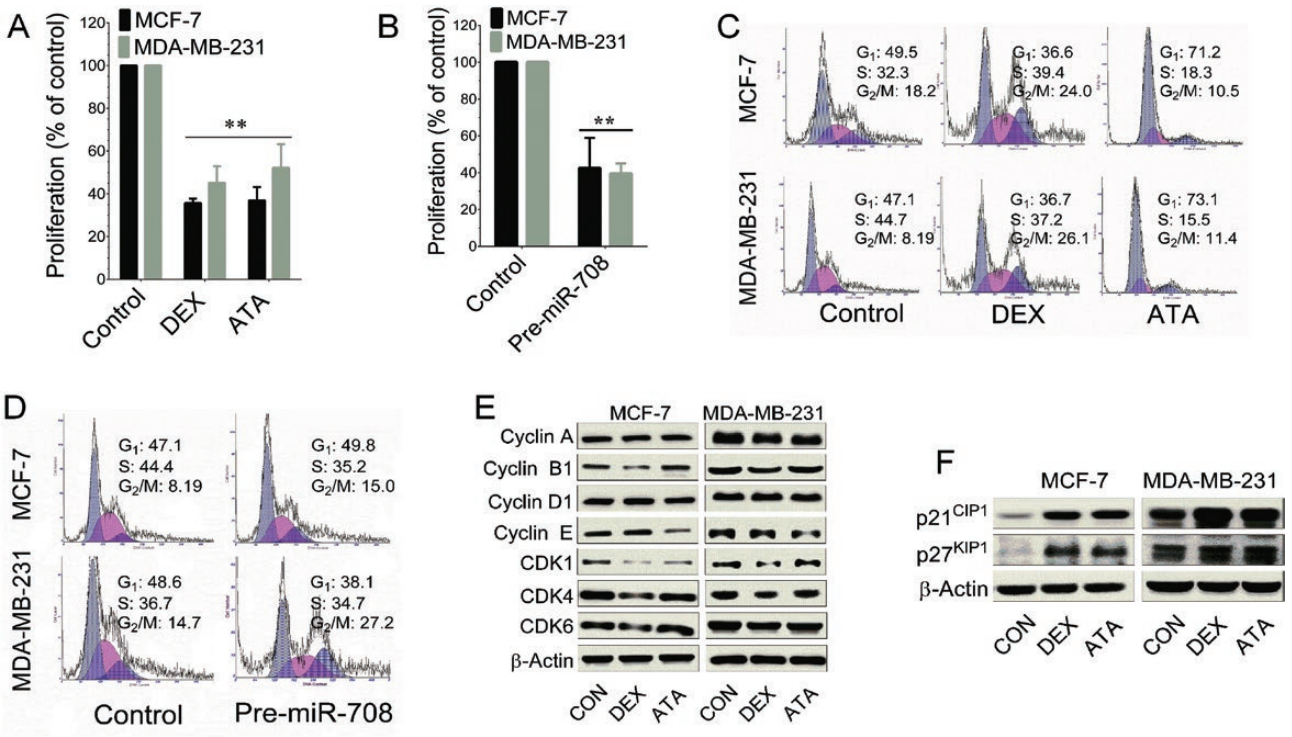

Figure 2. MiRNA-708/GRα axis inhibits proliferation of BCCs. **(A)** BCC proliferation after treatment with DEX or ATA for 72 h was measured by commercially available proliferation assay kit. **(B)** BCC proliferation after transfection with pre-miR-708 for 72 h. **(C)** BCCs were incubated with DEX or ATA for 72 h. Cell-cycle distribution was measured by a flow cytometer using PI. **(D)** BCCs were transfected with pre-miR-708 for 72 h. **(E)** Western blot analysis was performed to determine the expression levels of cell-cycle regulatory proteins after treatment with DEX or ATA for 72 h. **(F)** The protein expression levels of CDK inhibitors were determined by immunoblotting. β-Actin served as an internal control. The data are reported as mean ± SD of three independent experiments. **$P < 0.01$ was significantly different from the control versus pre-miR-708 transfection or DEX and ATA treatment groups.

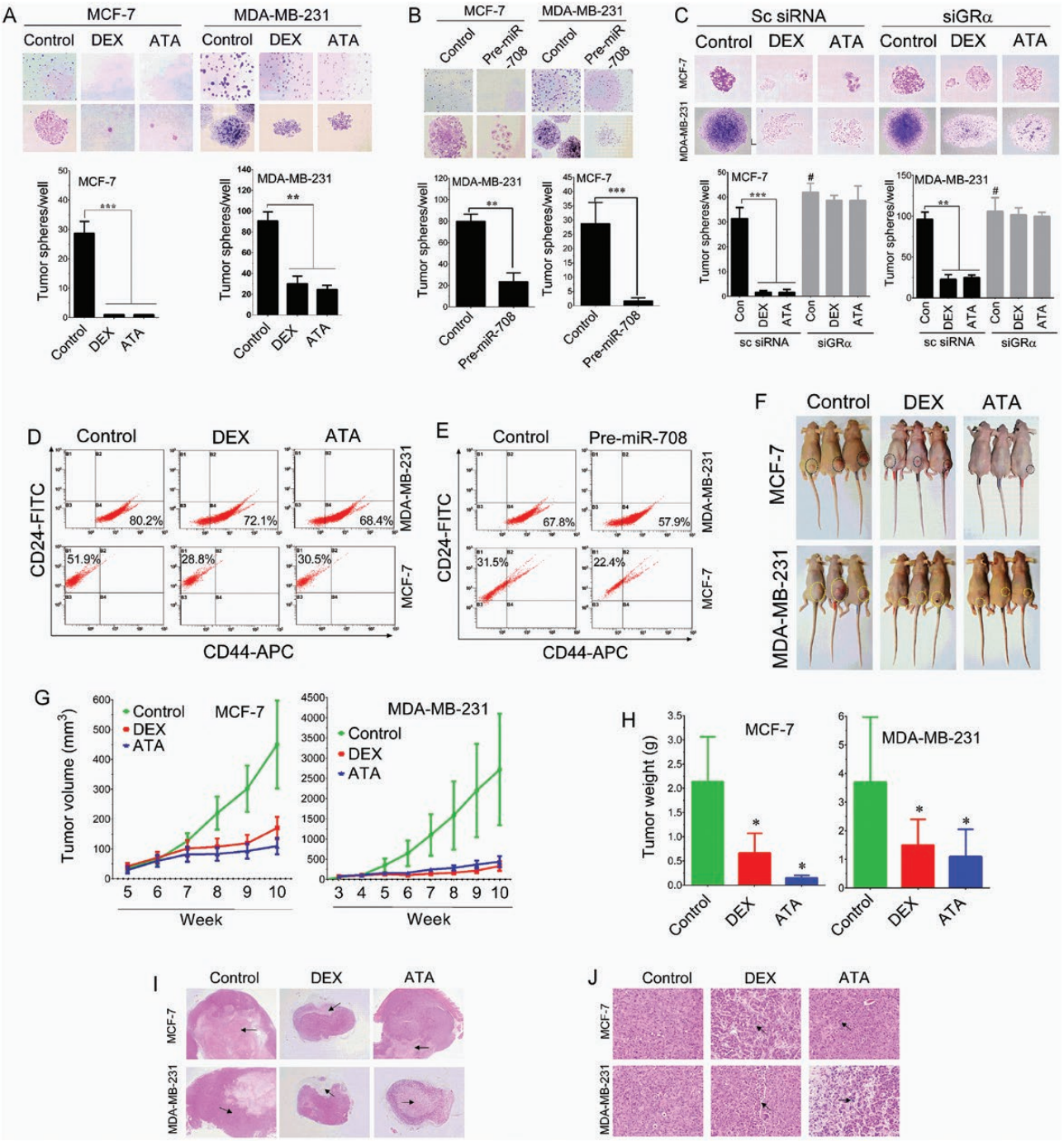

Figure 3. MiRNA-708/GRα axis regulates tumorigenesis *in vitro* and *in vivo*. **(A)** BCCs were seeded onto six-well plates. Each well contained 200 cells. After the cells settled, they were treated with DEX or ATA for 14 days. Tumor-sphere formation was observed and counted for each well. Number of tumor spheres in each well is shown in the histogram. **(B)** Number of tumor spheres was determined after transfection with pre-miR-708 for 14 days. **(C)** Tumor sphere formation in BCCs transfected with scrambled siRNA (sc siRNA) or siRNA specific to GRα (siGRα) and then incubated with DEX or ATA for 14 days. **(D** and **E)** After treatment with DEX or ATA or transfection with pre-miR-708 for 72 h, a flow cytometry-assisted cell sorting analysis was conducted using specific surface markers for MDA-MB-231 (CD44-APC) and MCF-7 cells and the percentage of cells ($CD44^+/CD24^+$) of each cell line was evaluated in three independent experiments. **(F)** BCC tumor xenograft growth in athymic mice with or without DEX or ATA treatment for 7 weeks. **(G)** Tumor volumes were measured at the end of the treatment (10 weeks). **(H)** Tumor weight was measured at end of the treatment. **(I)** Histological examination of the tumor xenograft showed tumor cell necrosis. **(J)** Histological examination of the tumor xenograft showed tumor cell apoptosis (H&E; magnification, ×100). The data are reported as mean ± SD of three independent experiments. $^*P < 0.05$, $^{**}P < 0.01$ and $^{***}P < 0.001$ were significantly different from control versus pre-miR-708 transfection or DEX and ATA treatment groups.

after 7 and 5 days, respectively (Figure 3A). MCF-7 cells formed five to seven tumor spheres per well under control conditions, whereas tumor spheres were not found in DEX- and ATA-treated cells. On the other hand, MDA-MB-231 cells formed 15–22 tumor spheres per well, whereas DEX- and ATA-treated cells significantly reduced tumor sphere formation to 5–7 tumor spheres and 3–7

tumor spheres, respectively. These data suggest that GR agonists effectively inhibited tumor-sphere formation in the BCCs tested. To further clarify the involvement of miR-708 in the inhibitory effects of GR agonists, tumor sphere formation was examined after transfection with pre-miR-708. As shown in Figure 3B, compared with untreated control cells, miR-708 overexpression clearly decreased the number of tumor spheres in both MCF-7 and MDA-MB-231 cells. We also found that treatment with DEX or ATA failed to inhibit tumor sphere formation in GRα-silenced cells (Figure 3C), suggesting that the *in vitro* anti-tumorigenic effects of GR agonists were mediated by the miR-708/GRα signaling cascade. To further evaluate whether DEX or ATA treatment could suppress breast CSCs *in vitro*, MDA-MB-231 and MCF-7 cells were incubated with DEX or ATA for 72 h. Then, we assessed the proportion levels of the prospective CSC markers $CD44^+$ and $CD24^+$ by fluorescence-activated cell sorting assay with CD44-APC and CD24-FITC conjugated antibodies. We found that both MDA-MB-231 and MCF-7 cells showed significantly reduced percentage of $CD44^+$ and $CD24^+$ cells, respectively, during treatment with DEX and ATA (Figure 3D). Similarly, transfection of pre-miR-708 exhibited significantly greater proportion of $CD44^+$ and $CD24^+$ cells in MDA-MB-231 and MCF-7, respectively (Figure 3E). Furthermore, western blot analysis also supporting the notion that treatment with DEX and ATA or transfection of pre-miR-708 significantly decreased the membrane bound CD44 and CD24 protein expression levels in MDA-MB-231 and MCF-7 cells, respectively (Supplementary Figure 6, available at *Carcinogenesis* Online). These data suggesting that the inhibition of tumor sphere formation by DEX and ATA or pre-miR-708 were strongly correlated with the downregulation CD44 and CD24 surface markers.

GR agonists inhibit BCC tumor growth in a xenograft animal model

The results of the *in vitro* tumorigenic assays outlined above revealed that GR agonists were potentially anti-tumorigenic agents. To validate these effects *in vivo*, MCF-7 and MDA-MB-231 cells were subcutaneously inoculated into the right flank of female athymic mice to develop breast tumor xenograft. After the tumor size reached 50 cm^3, mice received intraperitoneal injection of DEX and ATA twice a week for 10 weeks. As shown in Figure 3F and G, the tumor volume of vehicle groups increased aggressively after 5 weeks from 40 cm^3 to 450 mm^3 in mice bearing MCF-7 tumors and from 60 mm^3 to 2700 cm^3 in MDA-MB-231 tumors. However, treatment with DEX and ATA for 10 weeks significantly slowed the tumor growth as indicated by the tumor volume being reduced to 170 ± 37 and 110 ± 28 mm^3 in MCF-7 tumors and 330 ± 117 and 437 ± 136 mm^3 in MDA-MB-231 tumors, respectively. In addition, the tumor weight was measured at end of the experiment. The tumor weight of the control group of mice bearing MCF-7 tumors was 3.1 ± 0.5 g, and MDA-MB-231 inoculated mice had a tumor weight of 3.7 ± 1.3 g. Whereas treatment with DEX and ATA significantly decreased the tumor weight to 0.6 ± 0.2 and 0.15 ± 0.02 g in MCF-7-inoculated mice and 1.5 ± 0.5 and 1.1 ± 0.5 g in MDA-MB-231-inoculated mice, respectively (Figure 3H). Furthermore, we also found that ATA treatment slightly reduced mouse body weight although there was no visible adverse effect. Less than 10% body weight reduction was observed in the ATA-treated groups. Histopathological findings showed that a slight level of necrosis was found in the control groups, whereas massive necrotic regions were seen with DEX and ATA treatment groups of both mice bearing MCF-7 and MDA-MB-231 tumors (Figure 3I). Histochemical staining also showed no observable nuclear condensation or apoptotic bodies in the control groups, whereas DEX and ATA treatment groups of both MCF-7 and MDA-MB-231-bearing tumors exhibited increased levels of nuclear condensation as well as apoptotic bodies (Figure 3J). These data were a contradiction of the above observations that DEX or ATA do not induce apoptotic cell death in BCCs *in vitro*.

GR agonists inhibit migratory and invasive potential of BCCs *in vitro*

To further examine the functions mediated by GR agonists, we examined the antimetastatic potential of GR agonists by determining BCC migration and invasion in the presence of DEX and ATA. Since, the MCF-7 cells are poorly metastatic, TGF-β1 was added to the culture media to induce metastasis of MCF-7 cells (MCF-$7^{TGF\text{-}\beta}$). As shown in Figure 4A, compared with the untreated control cells, a remarkable increase in cell migration was observed in TGF-β1-treated cells, whereas treatment with DEX or ATA significantly reduced the TGF-β1-induced cell migration as evidenced by the percentage of wound closure being significantly decreased in DEX- or ATA-treated cells. Similarly, treatment with GR agonists, DEX and ATA, remarkably decreased the migratory potential of BCCs (Figure 4A). Indeed, a dose–response curve of DEX and ATA on tumor cell migration revealed that the highest dose of DEX (1 μM) and ATA (10 μM) only exhibits inhibitory effects (Supplementary Figure 6, available at *Carcinogenesis* Online). Next, *trans*-well invasion assay was conducted to determine whether GR agonists are able to block TGF-β1-induced invasion in MCF-7 cells. Figure 4B shows that the number of invasive cells in the TGF-β1 group was markedly higher than in the control group; however, a reduced number of invasive cells were observed in DEX- or ATA-treated MCF-$7^{TGF\text{-}\beta}$ cells. In addition, GR agonists significantly decreased the invasiveness of MDA-MB-231 cells, supported by the numbers of invading cells, which were significantly decreased after treatment with DEX and ATA (Figure 4B). Next, we hypothesized that inhibition of migration and invasion by GR agonists may be associated with downregulation of matrix metalloproteinases (MMPs); thus, MMP-2 and MMP-9 expression levels were determined. As we expected, the mRNA expression levels of MMP-2 and MMP-9 were significantly decreased by DEX and ATA in both MCF-7TGF-β and MDA-MB-231 cells (Figure 4C). To further confirm this effect, protein expression levels of MMP-2 and MMP-9 were examined. In parallel, the protein expression levels of MMP-2 and MMP-9 were markedly inhibited by DEX and ATA (Figure 4D). To further validate the metastasis regulatory function of GRα in BCCs, GRα was silenced in MCF-$7^{TGF\text{-}\beta}$ and MDA-MB-231 cells by transfection of siRNA specific to GRα and the anti-metastatic effects of DEX and ATA were determined by migration assay. As shown in Figure 4E, treatment with DEX or ATA significantly decreased the tumor cell migration in scrambled siRNA transfected cells, whereas DEX failed to inhibit the migration of MCF-$7^{TGF\text{-}\beta}$ and MDA-MB-231 cells. Interestingly, treatment with ATA partially inhibited tumor cell migration in GRα silenced cells, suggesting that ATA may also regulate other signaling pathways to control the tumor cell metastasis.

MiRNA-708/GRα axis specifically regulates IKKβ expression in BCCs

To identify the target genes of miR-708 that regulates breast cancer proliferation, three target prediction algorithms

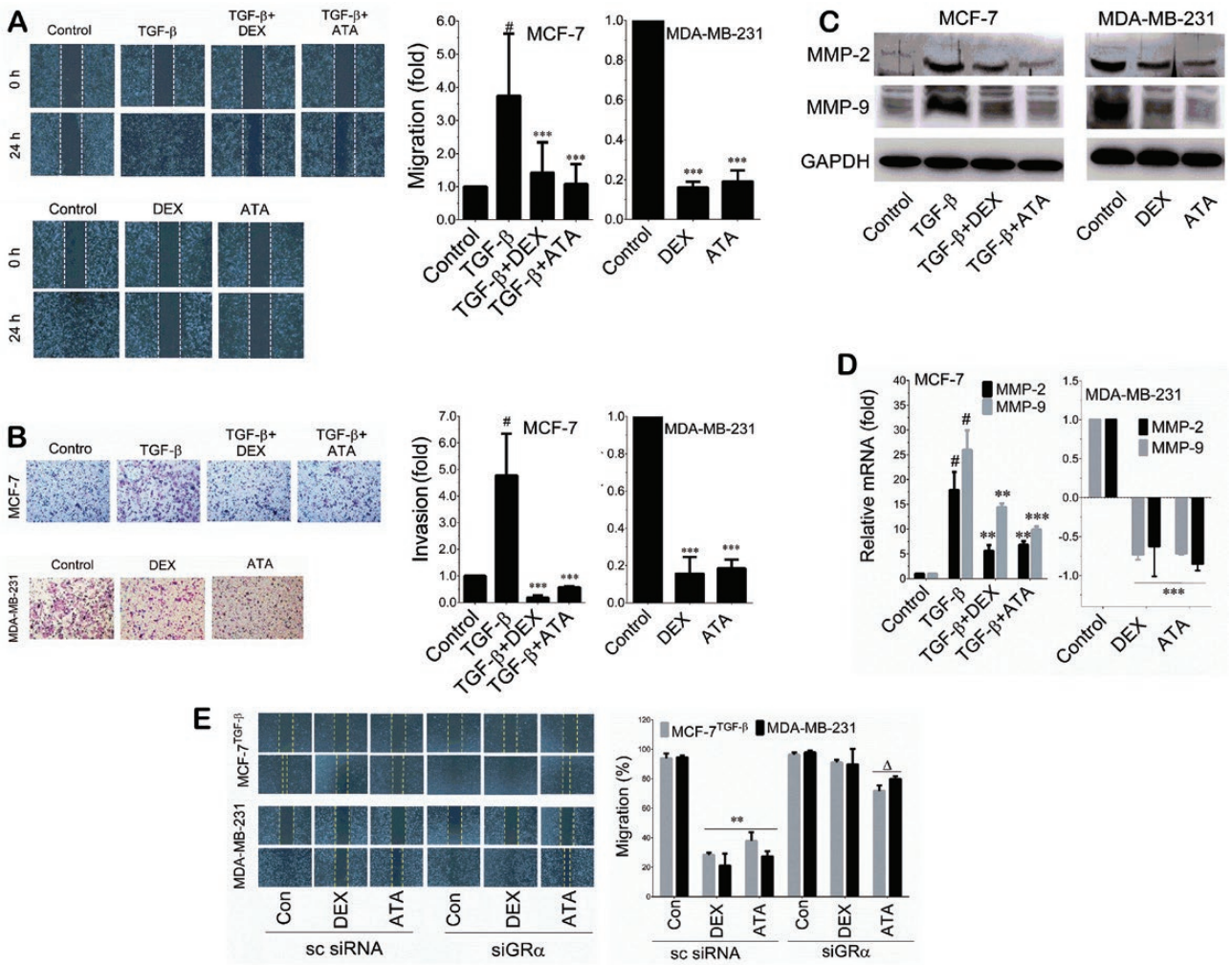

Figure 4. GR agonists inhibit BCC metastasis *in vitro*. **(A)** BCCs were treated with DEX or ATA for 24 h in the presence or absence of TGF-β. Cell migration was determined by wound healing assay, and the fold increase of tumor cell migration is shown in the histogram. **(B)** Tumor cell invasion was determined by transwell chamber assay after treatment with DEX or ATA in the presence or absence of TGF-β for 24 h. Photographs were taken at 0 and 248 h using an inverted microscope with ×10 magnification. **(C)** Protein expression levels of MMP-2 and MMP-9 were determined by western blot analysis with specific antibodies. **(D),** The mRNA expression levels of MMP-2 and MMP-9 were measured by Q-PCR. **(E)** BCC migration after transfection with scrambled siRNA (sc siRNA) or siRNA specific to GRα (siGRα) and then incubated with DEX or ATA for 24 h. The percentage of tumor cell migration is shown in the histogram. The data are reported as mean ± SD of three independent experiments. $^{\#}P < 0.001$, significant difference from control versus TGF-β1-treated group. $^{**}P < 0.01$ and $^{***}P < 0.001$ were significantly different from TGF-β1 alone with the DEX or ATA treatment groups. $^{\Delta}P < 0.001$, significant difference from siGRα transfection alone with the DEX or ATA treatment groups.

(miRanda, TargetScan and miRTarBase) were applied to search for mRNAs that interact with miR-708. All three algorithms suggested that miR-708 could target the NF-κB activating kinases beta (IKKβ). We focused on IKKβ, not only inspired by the target prediction algorithm but also because IKK–NF-κB is regarded as an important factor in breast carcinogenesis and a potential target for breast cancer therapy (24). The predicted binding site between inhibitor of NF-κB kinase subunit beta (IKBKB) and miR-708 is shown in Figure 5A. To assess the direct interaction of miR-708 with IKKβ, the 3′UTR region of IKKβ was cloned into a reporter plasmid downstream of firefly luciferase. Luciferase activity was reduced to 38.7 and 40.1% of the control in MCF-7 and MDA-MB-231, respectively, upon miR-708 transfection (Figure 5B). These data strongly suggest that IKKβ is a direct target of miR-708. Then, we analyzed the mRNA levels of the IKK subunits including IKKα, IKKβ and IKKγ in BCCs. Overexpression of miR-708 by pre-miR-708 resulted in a significant decrease of endogenous levels of IKKβ mRNA in both MCF-7 and MDA-MB-231 cells, whereas the mRNA levels of IKKα and IKKγ were unaffected by pre-miR-708 (Figure 5C). Similarly, treatment with GR agonists, DEX and ATA significantly downregulated IKKβ mRNA levels, whereas IKKα and IKKγ were unaffected (Figure 5D). These data strongly suggest that the reduction in IKKβ by GR agonists was mediated by miR-708. Further immunoblotting analyses revealed that treatment with DEX and ATA not only decreased IKKβ levels but also suppressed its phosphorylation, whereas either DEX or ATA treatment did not affect IKKα protein expression and its phosphorylation (Figure 5E). To further test the involvement of GRα in IKKβ regulation, BCCs were transiently transfected with GRα siRNA, and the protein and mRNA levels of IKKβ were examined. In GRα knockdown cells, both DEX and ATA failed to downregulate IKKβ mRNA (Figure 5F) and protein (Figure 5G) levels, whereas treatment with ATA significantly inhibited IKKβ phosphorylation even in GRα-silenced MDA-MB-231 cells, suggesting that inhibition of IKKβ phosphorylation is partially GRα independent. Together these findings demonstrate that IKKβ is a direct target of miR-708, which is activated by GR agonists.

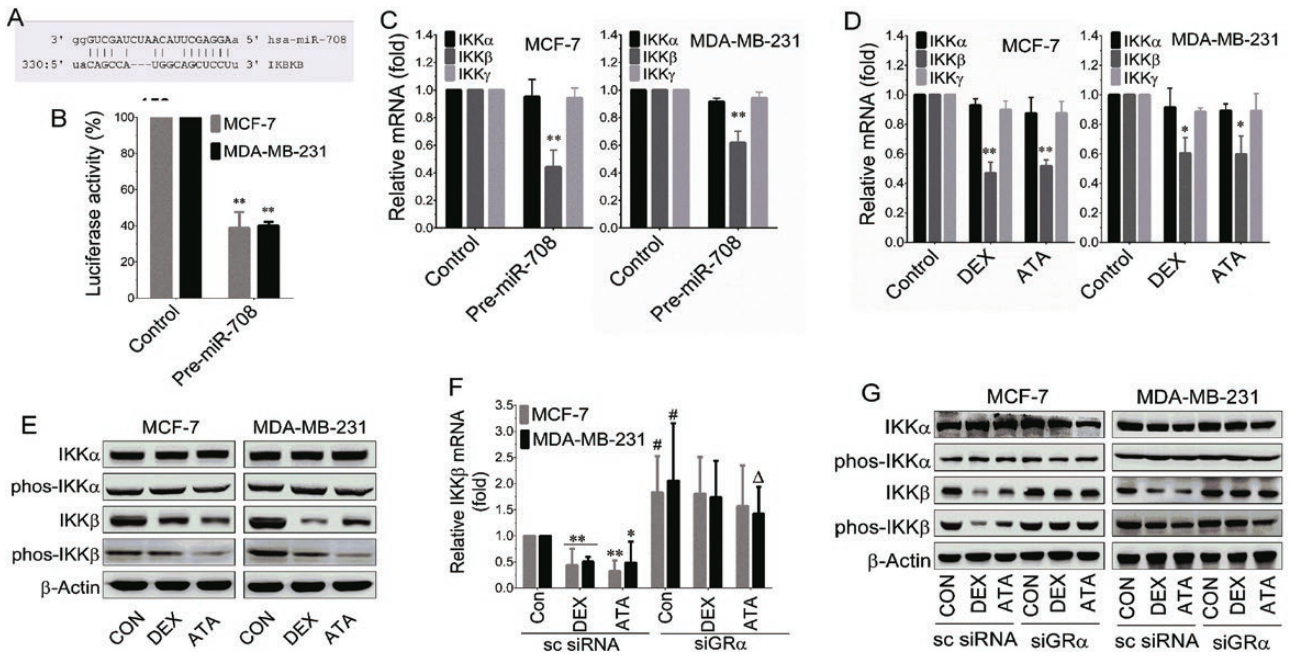

Figure 5. MiRNA-708/GRα axis specifically regulates IKKβ expression in BCCs. **(A)** The MiR-708 target site in the IKBKB (IKKβ) 3′UTR. **(B)** Promoter activity of IKKβ in BCCs after transfection with pre-miR-708 for 48 h (RLU, relative luciferase unit). **(C)** The mRNA expression levels of IKK subunits in BCCs after transfection with pre-miR-708 for 48 h. **(D)** The mRNA expression levels of IKK subunits in BCCs after treatment with DEX or ATA for 48 h. **(E)** IKKα and IKKβ protein expression and their phosphorylation levels were determined by western blotting. **(F)** IKKβ mRNA level after transfection with scrambled siRNA (sc siRNA) or siGRα and then incubation with DEX or ATA for 48 h. **(G)** IKKα and IKKβ protein expression level after transfection with scrambled siRNA (sc siRNA) or siGRα and then incubation with DEX or ATA for 48 h. The data are reported as mean ± SD of three independent experiments. $^{*}P < 0.05$ and $^{**}P < 0.01$ were significantly different from control versus pre-miR-708 transfection or DEX and ATA treatment groups. $^{\Delta}P < 0.001$, significant difference from siGRα transfection alone with the DEX or ATA treatment groups.

MiRNA-708 suppressed NF-κB activities in BCCs

NF-κB signaling has been identified in many cancer types and regulates the transcription of a wide range of genes that promote cell survival and proliferation, inhibit apoptosis, and induce CSC differentiation and tumor cell metastasis (13,25). A recent study (18) demonstrated that epigenetic silencing of miR-708 enhances NF-κB signaling in chronic lymphocytic leukemia. In view of the observed functions of miR-708 on proliferation, tumorigenesis and metastasis, we sought to examine whether miR-708 regulated cancer cells through NF-κB. Expression of miR-708 in the BCCs resulted in significant decrease of NF-κB transcriptional activity as evidenced by reduced luciferase reporter activity (Figure 6A). In addition, treatment with GR agonists, DEX and ATA significantly inhibited the transcriptional activation of NF-κB in BCCs (Figure 6B). Next, we examined the nuclear export of NF-κB under pre-miR-708 treatment. Western blot analysis showed that predominant expression of NF-κB was found in the nuclear fraction of control cells, whereas increased cytoplasmic NF-κB was found in pre-miR-708-transfected cells (Figure 6C). Similarly, treatment with DEX and ATA significantly blocked NF-κB nuclear translocation as indicated by lower levels of NF-κB in the nuclear fractions (Figure 6D). It has been reported previously that induction of GR suppressed NF-κB activity in HeLa cells (26). Therefore, we hypothesized that GR agonists mediating downregulation of IKKβ may play a functional role in suppression of NF-κB activity in BCCs. In order to validate this hypothesis, the transcriptional activity of NF-κB in GRα-silenced cells was determined. As shown in Figure 6E, treatment with DEX and ATA significantly inhibited NF-κB activity in scrambled siRNA-transfected cells, whereas DEX and ATA failed to inhibit NF-κB activity in GRα-silenced cells. Further analysis with immunoblotting showed that DEX- and ATA-mediated suppression of NF-κB nuclear translocation was barely observed in GRα-silenced cells (Figure 6F). To further clarify the effects of GR agonists on NF-κB regulation *in vivo*, BCCs bearing tumor tissues were subjected to immunohistochemical analysis. As indicated in Figure 6G, cells positively immune-stained for NF-κB were detected in tissues from the control groups; however, the number of NF-κB-positive immune-stained cells were significantly reduced by DEX and ATA treatment.

IKK phosphorylates NF-κB-bound inhibitor-κBs (I-κBs) at two conserved serines within the I-κB N-terminal regulatory domain. Degradation of I-κB proteins *via* phosphorylation and the ubiquitination-dependent pathway is an essential step for NF-κB activation. I-κB phosphorylation depends mainly on the IKKβ catalytic subunit of the IKK complex (10). Therefore, the upstream cascade of NF-κB, I-κBα was measured. As shown in Figure 6H, I-κB levels were barely observed in control cells, whereas increased levels of I-κB were observed in pre-miR-708-transfected cells. However, phosphorylation levels of I-κB were not observed in either the control or pre-miR-708 transfected cells. Treatment with DEX and ATA exhibited a similar trend of achieving I-κB protein stability after treatment (Figure 6I).

GR agonist-mediated activation of miR-708 represses NF-κB downstream target genes

Recent studies have reported that human breast carcinomas aberrantly express COX-2 and cMYC and raised levels of COX-2 and cMYC have prognostic value in patients with breast cancer (27,28). To test the downstream transcriptional effects of miR-708 on NF-κB signaling, expression of COX-2 and cMYC, which are well-known NF-κB target genes, was evaluated following tumor necrosis factor-α induction. Overexpression of miR-708 by pre-miR-708 induced impairment of the expression of COX-2

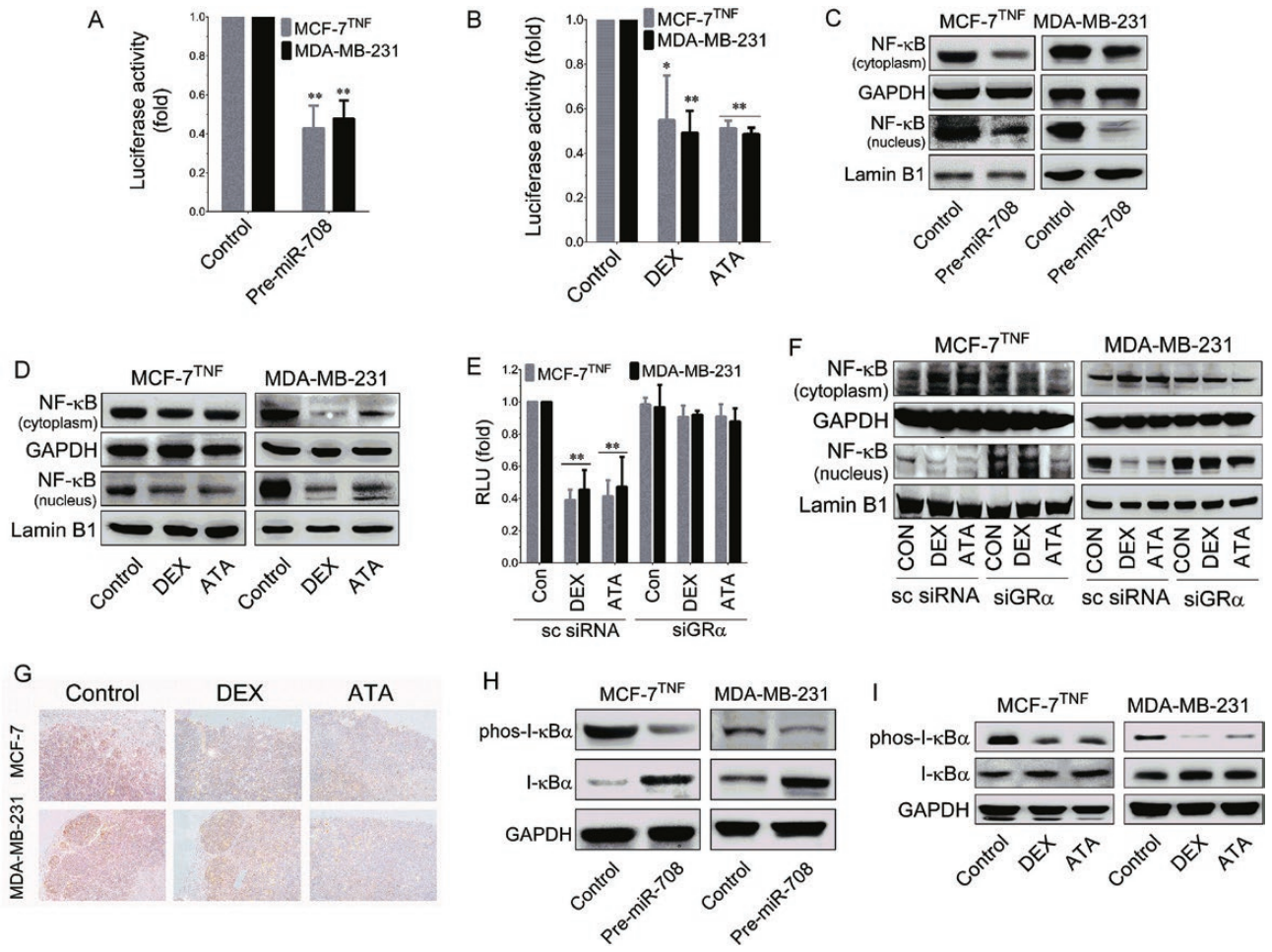

Figure 6. MiRNA-708 suppressed NF-κB activities in BCCs. **(A)** Luciferase activity of NF-κB in BCCs after transfection with pre-miR-708 for 48 h (RLU, relative luciferase unit). **(B)** Luciferase activity of NF-κB in BCCs after treatment with DEX or ATA for 48 h. **(C)** The protein levels of NF-κB in the cytoplasm and the nucleus after transfection with pre-miR-708 for 48 h. **(D)** The protein levels of NF-κB in cytoplasm and the nucleus after treatment with DEX and ATA for 48 h. Glyceraldehyde 3-phosphate dehydrogenase and Lamin B1 served as internal controls for the cytoplasmic and nuclear fractions, respectively. **(E)** Luciferase activity of NF-κB after transfection with scrambled siRNA or siGRα and then incubation with DEX or ATA for 48 h. **(F)** The protein levels of NF-κB in the cytoplasm and the nucleus after transfection with scrambled siRNA or siGRα and then incubation with DEX or ATA for 48 h. **(G)** IHC staining of NF-κB in the tumor xenograft after treatment with vehicle control or DEX or ATA. **(H)** The protein levels of I-κBα and its phosphorylation in BCCs after transfection with pre-miR-708 for 48 h. **(I)** Protein levels of I-κBα and its phosphorylation in BCCs after treatment with DEX or ATA for 48 h. To induce the NF-κB signaling in MCF-7 cells, cells were pretreated with human tumor necrosis factor-α (10 ng/ml) and the tumor necrosis factor-α-stimulated MCF-7 cells were represented as MCF-7^{TNF}. The data are reported as mean ± SD of three independent experiments. **$P < 0.01$ was significantly different from control versus pre-miR-708 transfection or DEX and ATA treatment groups.

and cMYC genes at both the transcriptional (Figure 7A) and translational (Figure 7B) levels. A similar result was observed in GR agonists, DEX- and ATA-treated cells (Figure 7C). In addition, tumor tissues from *in vivo* experiments were subjected to IHC with the COX-2 antibody resulting in markedly fewer positively stained cells in the DEX- and ATA-treated groups compared with the vehicle treatment groups (Figure 7D). To evaluate the effect of GRα activation on COX-2 expression, RT-PCR was performed following DEX or ATA treatment in GRα-silenced cells. Results of RT-PCR analysis showed that compared with the control group, COX-2 gene was significantly increased in GRα-silenced cells. However, treatment with DEX and ATA partially inhibited COX-2 expression in GRα-silenced cells (Figure 7E).

Discussion

MicroRNA-708 is one of the most downregulated miRNAs in many cancer types, including renal cell carcinoma, prostate cancer, glioblastoma, hepatocellular carcinoma, ovarian carcinoma and breast carcinoma (17,29). In contrast, high expression of miR-708 was observed in non-small-cell lung carcinoma, childhood common precursor B-cell acute lymphocyte leukemia and bladder carcinoma (17,29). It was revealed that miR-708 was frequently observed in most metastatic tumor cells; however, its role in tumorigenesis has barely been explored. A previous study by Ryu *et al.* (30) reported that suppression of miR-708 by polycomb group promotes metastasis by calcium-induced cell migration in breast cancer and a following study (19) demonstrated that forced induction of miR-708 inhibits proliferation and invasion of BCCs *via* suppressing LSD1. Since miR-708 is highly conserved across species, and differentially expressed in specific tissues, we initially examined the miR-708 expression levels in a panel of non-tumorigenic, tumorigenic (non-metastatic) and tumorigenic (metastatic) breast cells. Results showed high expression of miR-708 in non-tumorigenic MCF-10A cells, whereas miR-708 was markedly suppressed in tumorigenic with metastatic cells compared with tumorigenic with non-metastatic cells. Additionally, we

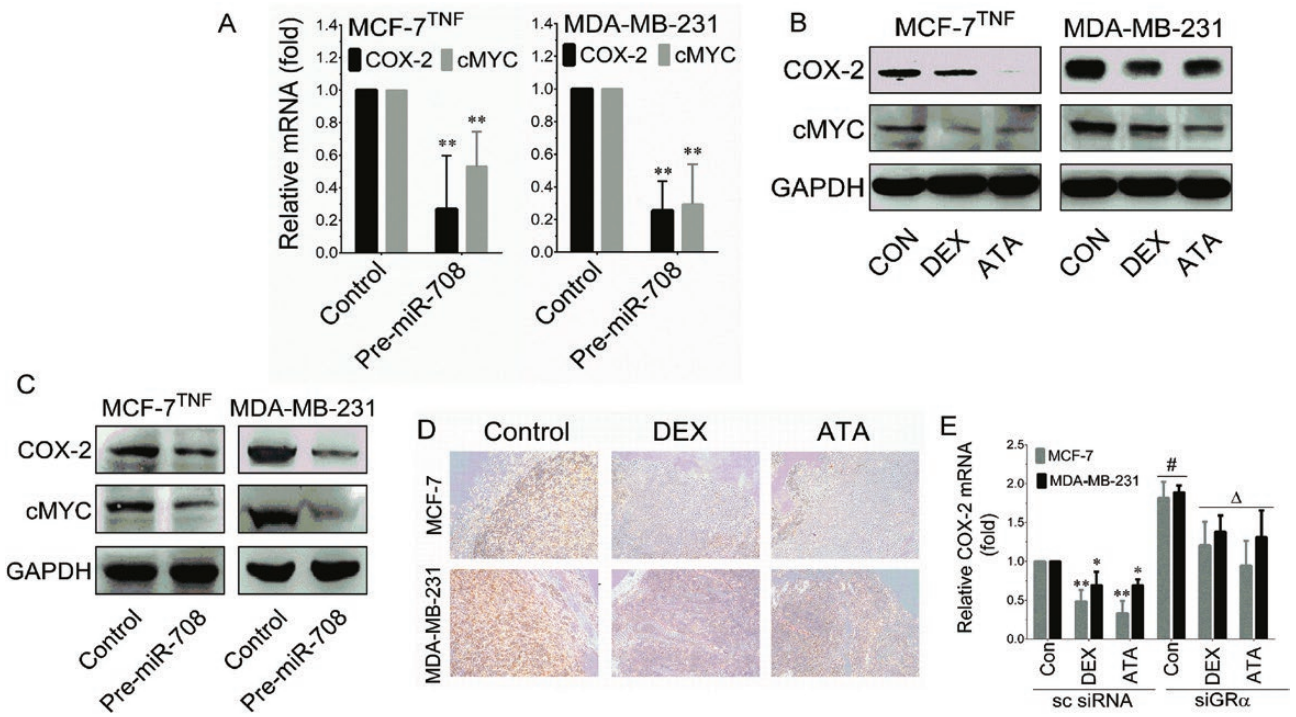

Figure 7. GR agonist-mediated activation of miR-708 represses NF-κB downstream target genes. **(A)** The mRNA expression levels of COX-2 and cMYC in BCCs after transfection with pre-miR-708 for 48 h. **(B)** COX-2 and cMYC protein levels were determined by western blotting after transfection with pre-miR-708 for 48 h. **(C)** The protein expression levels of COX-2 and cMYC in BCCs after treatment with DEX or ATA for 48 h. **(D)** IHC staining of COX-2 in tumor xenograft after treatment with vehicle control or DEX or ATA. **(E)** COX-2 mRNA level after transfection with scrambled siRNA (sc siRNA) or siGRα and then incubation with DEX or ATA for 48 h. The data are reported as mean ± SD of three independent experiments. $^{**}P < 0.01$ was significantly different from control versus pre-miR-708 transfection or DEX and ATA treatment groups. $^{\#}P < 0.05$, significant difference from sc siRNA control versus siGRα control. $^{\Delta}P < 0.001$, significant difference from siGRα transfection alone with the DEX or ATA treatment groups.

found that forced expression of miR-708 by transfection with its precursor significantly inhibited BCC proliferation and *in vitro* tumorigenicity, which is concomitant with the observations of others in BCCs (19) or other cancer cells (31–33). The inhibition of cell proliferation by miR-708 mimic was found to be through cell-cycle arrest. However, the growth arrest was different in metastatic and non-metastatic cells; in MCF-7 cells, miR-708 mimic arrests cells at G_1-S transition and in MDA-MB-231 cells arrest occurs at the G_2-M transition. Further examination with cell-cycle regulatory proteins revealed that miR-708 mimic induced $p21^{CIP1}$ and $p27^{KIP1}$ in both cell lines. Collectively, our results demonstrated that miR-708 function as an anti-tumor factor in breast cancer.

An accumulating body of evidence showed that miRNAs regulate the properties of embryonic stem cells and tissue stem cells in a variety of eukaryotic organisms. Recent discoveries of miRNA have provided a new direction for understanding the regulatory mechanisms in CSCs. A previous study by Shimono *et al.* (34) found that in breast CSCs, eight miRNAs are selectively downregulated and located on the three miRNA clusters, such as miR-200c-141, miR-200b-200a-429 and miR-183-96-182 and two of the three clusters are the miR-200 clusters (miR-200c-141 and miR-200b-200a-429). Expression of BMI1, a known regulator of stem cell self-renewal, was modulated by miR-200c, suggesting that the suppression of the miR-200 family is critically important in the maintenance of stem cell function (35). In addition, upregulation of let-7 family miRNAs targets H-RAS and HMGA2 and suppresses self-renewal and differentiation of breast CSCs (36). This evidence suggests that breast CSC-specific miRNAs play important roles in the regulation of self-renewal ability, tumorigenicity, and metastasis. In the present study, we selected the highly aggressive BCC line, MDA-MB-231 to examine the potential effects of GR agonists or miR-708 on CSCs. MDA-MB-231 is a TNBC, i.e. $ER^-/PR^-/HER\text{-}1^-$, highly metastatic with a high proportion of $CD44^+/CD24^{-/-}$population. As the MDA-MB-231 cell line possess a high $CD44^+$ cell population, it serves as a good model for breast CSCs. To investigate the effects of GR agonists and miR-708 overexpression on breast CSCs, we employed the tumor-sphere formation assay to characterize the CSCs. We found that treatment with either GR agonist or transfection of miR-708 mimics significantly decreased tumor sphere formation and $CD44^+$ expression, suggesting that activation of miR-708 by GR agonists suppress CSC-like phenotype in BCCs.

Previous studies have presented controversial results in the use of GR agonists in cancer treatment. The synthetic GR agonist DEX suppressed small-cell lung carcinoma and breast cancer tumor growth via increasing estrogen sulfotransferase and decreasing estradiol in tumor tissues (37). A recent study by Lin et al. reported that GR agonist, DEX activates miR-708 to suppress ovarian cancer metastasis by targeting Rap1B (23). Therefore, we hypothesize that the GR agonist may upregulate miR-708, which may have the potential to suppress tumorigenicity of BCCs. Here, we found that treatment with synthetic GR agonist, DEX or naturally occurring GR agonist ATA, reduced BCC proliferation and colony formation, and induced cell-cycle arrest through the induction of miR-708. Interestingly, we also observed that either synthetic or natural GR agonists do not induce apoptosis in tested BCCs, which is in contradiction to a previous observation in acute lymphoblastic leukemia (38). A previous study demonstrated that GR antagonist mifepristone had no effect on TNBC cells viability

or colonogenecity in the absence of chemotherapeutic drug Paclitaxel, whereas addition of mifepristone to DEX/Paclitaxel treatment significantly increased cytotoxicity (8). Several studies have demonstrated that DEX at a concentration of 100 nM induce proliferation of TNBC cells, whereas the effects of DEX on >100 nM was poorly illustrated. In the present study, we reported that over a dose of 500 nM DEX significantly inhibited TNBC cell proliferation without affecting GRα, as evidenced by increased levels of miR-708 in MDA-MB-231 cells. This effect was in agreement with a recent study that treatment with DEX (100 nM) inhibits proliferation of MDA-MB-231 cells *in vitro* (39). In addition, the anti-proliferative effects of DEX and ATA were extended to *in vivo* that GR agonists significantly reduced growth, weight and volume of MCF-7 and MDA-MB-231 BCC xenograft of nude mice. These results show the potential of GR agonists in breast cancer therapy.

Tumor cell migration and invasion are critical components of metastasis. Therefore, we examined the effects of GR agonists on migration and invasive behaviors of BCCs. We found that both migration and invasive potential of MDA-MB-231 and MCF-7^{TGF} cells were significantly inhibited by DEX and ATA *in vitro*. This observation was in agreement with a previous study that treatment with DEX (100 nM) inhibits migration and invasive potential of MDA-MB-231 cells, whereas this concentration failed to inhibit highly metastatic variant MDA-MB-231-HM. LNm5 cells (40). In contrast, data from our study exhibit that 100 nM of DEX failed to inhibit migration of MDA-MB-231 cells, whereas over a concentration of 100 nM significantly inhibited migration of MDA-MB-231 cells.

In human breast cancer, the NF-κB pathway is hyperactive and provides a pro-survival function. The NF-κB signaling pathway responds to different stimuli, from cytokine and growth factor signaling to the recognition of pathogen products or DNA damage and oncogenic stress (41). Studies with pharmacological inhibitors showed increased apoptosis of BCCs *in vitro* and reduced tumor growth *in vivo* (42,43). The activation of the canonical NF-κB signaling pathway occurs via inducing its upstream kinases IKKα and IKKβ that facilitate proteosomal degradation of the inhibitory proteins I-κBα/β allowing NF-κB nuclear translocation and subsequent transcriptional activation (41). Numerous signaling pathways that activate NF-κB converge at the level of IKKβ, including growth factors, inflammatory cytokines, endotoxins and viral infection. The activated NF-κB is not only involved in immune and inflammatory response but also in regulating adhesion, angiogenesis, autophagy, energy metabolism, senescence, and inducing cell proliferation and survival (44). It is, therefore, not surprising that NF-κB has been involved in cancer onset and progression both in experimental models and in human patients. In this study, we have predicted that miR-708 targets IKKβ, an upstream kinase of NF-κB. The luciferase reporter assay supports the prediction that miR-708 directly binds to the 3′UTR region of IKKβ. We also found that overexpression of miR-708 or treatment with GR agonists significantly reduced IKKβ protein expression as well as NF-κB transcriptional activity. In addition, treatment with GR agonists significantly reduced NF-κB expression in tumor tissues of BCC xenografted mice. Recently, others also demonstrated the NF-κB inhibitory function of miR-708 in chronic lymphocytic leukemia (18). Furthermore, recent studies indicate that mammary epithelial NF-κB regulates the self-renewal of breast CSCs (13) and pharmacological inhibition of NF-κB reduced self-renewal and blocked xenograft growth (45). Thus, we believe that GR agonists or miR-708 mimic-mediated inhibition of cancer-stem cell-like phenotype and the CD44+ cell population may be associated with suppression of the NF-κB signaling cascade. These results provide evidence that miR-708 and NF-κB closely interact in regulating growth and CSC-like phenotype of BCCs.

High COX-2 activity is a common feature of human epithelial tumors, including colorectal, breast and prostate (46). In breast cancer, the expression of COX-2 regulates tumor growth, invasion and metastasis, which suggests it may serve as a prognostic biomarker for the presence of breast cancer (28). Several COX-2 inhibitors on tumor cells have been shown to inhibit cancer cell proliferation and induce apoptosis (47). In addition, epidemiological studies have revealed that chronic exposure to non-steroidal anti-inflammatory drugs inhibits COX-2-mediated production of prostaglandins and is associated with a lower incidence of a number of cancers, including breast cancers (48) . Therefore, COX-2 inhibitors have been used clinically in combination with anti-cancer drugs (49). On the other hand, cMYC, is an oncogene that is highly expressed in most human cancers, including lymphoma, melanoma, myeloid leukemia, gastrointestinal, prostate and breast cancer (50). A previous study demonstrated that the overexpression of c-Myc by an inducible system in the mammary epithelium of transgenic mice resulted in the formation of invasive mammary adenocarcinomas, whereas inactivation of cMYC resulted in the sustained regression of tumors (51). To consider the significance of the role of COX-2 and cMYC in cancer prevention, and combination with anticancer drugs, we assessed the effects of GR agonists on COX-2 and cMYC expression in BCCs. Data from RT-PCR and immunoblotting showed that treatment with GR agonists or miR-708 mimic significantly downregulated COX-2 and cMYC gene and protein expression in both MCF-7 and MDA-MB-231 cells. Also, we found that treatment with GR agonists significantly inhibited COX-2 expression in xenograft tumors bearing MCF-7 or MDA-MB-231 cells.

In conclusion, the present study provides the first demonstration that synthetic or naturally derived GR agonists activate miR-708 through GRα, which inhibits proliferation and induces cell-cycle arrest in BCCs. Signaling mediated by GR agonists induces miR-708 expression, leading to the suppression of NF-κB, and the downregulation of its target genes COX-2 and cMYC. The present study implies the potential use of GR agonists or their downstream miRNA-708 regulation to inhibit breast cancer tumorigenesis.

Supplementary material

Supplementary Tables 1–3 and Figures 1–6 can be found at *Carcinogenesis* online.

Conflict of Interest Statement: None declared.

References

1. Jemal, A. *et al.* (2011) Global cancer statistics. CA Cancer J. Clin., 61, 69–90.
2. Ferlay, J. *et al.* (2015) Cancer incidence and mortality worldwide: sources, methods and major patterns in GLOBOCAN 2012. Int. J. Cancer, 136, E359–E386.
3. Schoneveld, O.J.L.M. *et al.* (2004) Mechanisms of glucocorticoid signalling. Biochim. Biophys. Acta., 1680, 114–128.
4. Becker, D.E. (2013) Basic and clinical pharmacology of glucocorticosteroids. Anesthes. Progres., 60, 25–32.
5. Chen, F.C. *et al.* (2017) Meta-analysis of the effects of oral and intravenous dexamethasone premedication in the prevention of paclitaxel-induced allergic reactions. Oncotarget, 8, 19236–19243.
6. Moon, E.Y. *et al.* (2014) Dexamethasone inhibits *in vivo* tumor growth by the alteration of bone marrow CD11b^{+} myeloid cells. Int. Immunopharmacol., 21, 494–500.

7. Lin, K.T. *et al.* (2016) New dimension of glucocorticoids in cancer treatment. Steroids, 111, 84–88.
8. Skor, M.N. *et al.* (2013) Glucocorticoid receptor antagonism as a novel therapy for triple-negative breast cancer. Clin. Cancer Res., 19, 6163–6172.
9. Sui, M. *et al.* (2006) Glucocorticoids interfere with therapeutic efficacy of paclitaxel against human breast and ovarian xenograft tumors. Int. J. Cancer, 119, 712–717.
10. Karin, M. *et al.* (2002) NF-kappaB in cancer: from innocent bystander to major culprit. Nat. Rev. Cancer, 2, 301–310.
11. Matsui, W.H. (2016) Cancer stem cell signaling pathways. Medicine (Baltimore)., 95 (1 Suppl 1), S8–S19.
12. Dandawate, P.R. *et al.* (2016) Targeting cancer stem cells and signaling pathways by phytochemicals: novel approach for breast cancer therapy. Semin. Cancer Biol., 40-41, 192–208.
13. Shostak, K. *et al.* (2011) NF-κB, stem cells and breast cancer: the links get stronger. Breast Cancer Res., 13, 214.
14. Huang, Y. *et al.* (2011) Biological functions of microRNAs: a review. J. Physiol. Biochem., 67, 129–139.
15. Croce, C.M. (2009) Causes and consequences of microRNA dysregulation in cancer. Nat. Rev. Genet., 10, 704–714.
16. Iorio, M.V. *et al.* (2005) MicroRNA gene expression deregulation in human breast cancer. Cancer Res., 65, 7065–7070.
17. Monteleone, N.J. *et al.* (2017) miR-708-5p: a microRNA with emerging roles in cancer. Oncotarget, 8, 71292–71316.
18. Baer, C. *et al.* (2015) Epigenetic silencing of miR-708 enhances NF-κB signaling in chronic lymphocytic leukemia. Int. J. Cancer, 137, 1352–1361.
19. Ma, L. *et al.* (2016) miR-708/LSD1 axis regulates the proliferation and invasion of breast cancer cells. Cancer Med., 5, 684–692.
20. Aldini, R. *et al.* (2014) Antiinflammatory effect of phytosterols in experimental murine colitis model: prevention, induction, remission study. PLoS One, 9, e108112.
21. Chen, Y.C. *et al.* (2011) Antcin A, a steroid-like compound from *Antrodia camphorata*, exerts anti-inflammatory effect via mimicking glucocorticoids. Acta Pharmacol. Sin., 32, 904–911.
22. Senthil, K.K. *et al.* (2016) A steroid like phytochemical Antcin M is an anti-aging reagent that eliminates hyperglycemia-accelerated premature senescence in dermal fibroblasts by direct activation of Nrf2 and SIRT-1. Oncotarget, 7, 62836–62861.
23. Lin, K.T. *et al.* (2015) Glucocorticoids mediate induction of microRNA-708 to suppress ovarian cancer metastasis through targeting Rap1B. Nat. Commun., 6, 5917.
24. Kendellen, M.F. *et al.* (2014) Canonical and non-canonical NF-κB signaling promotes breast cancer tumor-initiating cells. Oncogene, 33, 1297–1305.
25. Rinkenbaugh, A.L. *et al.* (2016) The NF-κB pathway and cancer stem cells. Cells, 5, 16.
26. Nelson, G. *et al.* (2003) NF-kappaB signalling is inhibited by glucocorticoid receptor and STAT6 via distinct mechanisms. J. Cell Sci., 116(Pt 12), 2495–2503.
27. Xu, J. *et al.* (2010) MYC and breast cancer. Genes Cancer, 1, 629–640.
28. Jana, D. *et al.* (2014) Role of cyclooxygenase 2 (COX-2) in prognosis of breast cancer. Indian J. Surg. Oncol., 5, 59–65.
29. Seven, M. *et al.* (2014) The role of miRNAs in cancer: from pathogenesis to therapeutic implications. Future Oncol., 10, 1027–1048.
30. Ryu, S. *et al.* (2013) Suppression of miRNA-708 by polycomb group promotes metastases by calcium-induced cell migration. Cancer Cell, 23, 63–76.
31. Jang, J.S. *et al.* (2012) Increased miR-708 expression in NSCLC and its association with poor survival in lung adenocarcinoma from never smokers. Clin. Cancer Res., 18, 3658–3667.
32. Guo, P. *et al.* (2013) miR-708 acts as a tumor suppressor in human glioblastoma cells. Oncol. Rep., 30, 870–876.
33. Lei, S.L. *et al.* (2014) Regulatory roles of microRNA-708 and microRNA-31 in proliferation, apoptosis and invasion of colorectal cancer cells. Oncol. Lett., 8, 1768–1774.
34. Shimono, Y. *et al.* (2016) MicroRNA regulation of human breast cancer stem cells. J. Clin. Med., 5, 2.
35. Shimono, Y. *et al.* (2009) Downregulation of miRNA-200c links breast cancer stem cells with normal stem cells. Cell, 138, 592–603.
36. Yu, F. *et al.* (2007) let-7 regulates self renewal and tumorigenicity of breast cancer cells. Cell, 131, 1109–1123.
37. Gong, H. *et al.* (2008) Glucocorticoids antagonize estrogens by glucocorticoid receptor-mediated activation of estrogen sulfotransferase. Cancer Res., 68, 7386–7393.
38. Laane, E. *et al.* (2007) Dexamethasone-induced apoptosis in acute lymphoblastic leukemia involves differential regulation of Bcl-2 family members. Haematologica, 92, 1460–1469.
39. Sperlich, J. *et al.* (2018) Pseudopterosin inhibits proliferation and 3D invasion in triple-negative breast cancer by agonizing glucocorticoid receptor alpha. Molecules, 23, 1992.
40. Fietz, E.R. *et al.* (2017) Glucocorticoid resistance of migration and gene expression in a daughter MDA-MB-231 breast tumour cell line selected for high metastatic potential. Sci. Rep., 7, 43774.
41. Fusella, F. *et al.* (2017) The IKK/NF-κB signaling pathway requires Morgana to drive breast cancer metastasis. Nat. Commun., 8, 1636.
42. Keane, M.M. *et al.* (2000) Inhibition of NF-kappaB activity enhances TRAIL mediated apoptosis in breast cancer cell lines. Breast Cancer Res. Treat., 64, 211–219.
43. Connelly, L. *et al.* (2011) Inhibition of NF-kappa B activity in mammary epithelium increases tumor latency and decreases tumor burden. Oncogene, 30, 1402–1412.
44. Xia, Y. *et al.* (2014) NF-κB, an active player in human cancers. Cancer Immunol. Res., 2, 823–830.
45. Song, L. *et al.* (2012) TGF-β induces miR-182 to sustain NF-κB activation in glioma subsets. J. Clin. Invest., 122, 3563–3578.
46. Xu, X.C. (2002) COX-2 inhibitors in cancer treatment and prevention, a recent development. Anticancer. Drugs, 13, 127–137.
47. Basu, G.D. *et al.* (2005) Mechanisms underlying the growth inhibitory effects of the cyclo-oxygenase-2 inhibitor celecoxib in human breast cancer cells. Breast Cancer Res., 7, R422–R435.
48. Harris, R.E. *et al.*; Women's Health Initiative. (2003) Breast cancer and nonsteroidal anti-inflammatory drugs: prospective results from the Women's Health Initiative. Cancer Res., 63, 6096–6101.
49. Bundred, N.J. *et al.* (2005) Potential use of COX-2-aromatase inhibitor combinations in breast cancer. Br. J. Cancer, 93 (Suppl 1), S10–S15.
50. Miller, D.M. *et al.* (2012) c-Myc and cancer metabolism. Clin. Cancer Res., 18, 5546–5553.
51. D'Cruz, C.M. *et al.* (2001) c-MYC induces mammary tumorigenesis by means of a preferred pathway involving spontaneous Kras2 mutations. Nat. Med., 7, 235–239.